

*Full Paper*

## **Reduced Graphene Oxide-Cr<sub>2</sub>O<sub>3</sub> Nanocomposite as Electrode Material in Supercapacitors**

**Kourosh Adib,<sup>1,\*</sup> Behnam Chameh,<sup>2</sup> and Fardin Gravand<sup>1</sup>**

<sup>1</sup>*Department of Chemistry, Faculty of Science, University of Imam Hossein, Tehran, Iran*

<sup>2</sup>*Materials and Energy Research Center (MERC), P.O. Box 31787-316, Karaj, Iran*

\*Corresponding Author, Tel.: +98-2177104936

E-Mail: [k\\_anbaz@yahoo.com](mailto:k_anbaz@yahoo.com)

*Received: 4 June 2020 / Received in revised form: 19 July 2020 /*

*Accepted: 20 July 2020 / Published online: 31 July 2020*

---

**Abstract-** In recent years, electrochemical supercapacitors have received considerable attention from many researchers. Metal oxides such as chromium oxide with high redox activity, high specific capacity, and excellent reversibility are suitable alternatives to ruthenium oxide in supercapacitor applications. In this study, first, graphene oxide (GO) was synthesized by the modified Hummers method. The synthesized GO was reduced using hydrazine hydrate (HH.rGO) and thermal reduction (Th.rGO). Also, chromium oxide (Cr<sub>2</sub>O<sub>3</sub>) was synthesized using a simple method. The synthesized compounds were characterized using the scanning electron microscope, infrared spectroscopy, and X-ray diffraction methods. Then Cr<sub>2</sub>O<sub>3</sub> and reduced GO were mixed in N-methyl pyrrolidone at a ratio of 20:80. Electrochemical properties of HH.rGO/Cr<sub>2</sub>O<sub>3</sub> and Th.rGO/Cr<sub>2</sub>O<sub>3</sub> nanocomposites were evaluated by cyclic voltammetry, electrochemical impedance spectroscopy, and chronopotentiometry methods. The supercapacitor studies show that the nanocomposites have excellent reversible supercapacitor behavior and suitable electrochemical performance. The specific capacity of HH.rGO/Cr<sub>2</sub>O<sub>3</sub> and Th.rGO/Cr<sub>2</sub>O<sub>3</sub> electrodes were 101 F/g and 151 F/g, respectively at the scan rate of 2 mV/s. These results indicate that the composition of Cr<sub>2</sub>O<sub>3</sub> with GO increases the specific capacity of supercapacitor due to the synergistic effect of GO and metal oxide.

**Keywords-** Supercapacitor; Nanocomposite; Reduced graphene oxide; Chromium oxide

---

## 1. INTRODUCTION

Supercapacitors, batteries, and fuel cells are the most important alternative energy sources for fossil fuels that do not have the environmental pollution caused by non-renewable fuels. Today, to achieve clean energy and use it in different industries, different countries are looking for this alternative energy and have considered it as one of their national development programs. Supercapacitors have several advantages compared to batteries. For example, the power density of batteries is  $150 \text{ W kg}^{-1}$  while the power density of supercapacitors is  $10 \text{ kW kg}^{-1}$ . Longer lifetime, low energy dissipation in the discharge cycle, and about 95% efficiency, better biocompatibility, and its application in a wide range of temperatures are among the advantages of supercapacitors over batteries [1-4].

What influences the performance of supercapacitors are the electrodes and active electrode materials which play an important role in the mechanism of energy storage in supercapacitors. Based on the mechanism of energy storage, the supercapacitors are divided into three categories which are electric double-layer capacitors, pseudocapacitors, and hybrid capacitors. Carbon materials, transition metal oxides, conductive polymers, and conductive polymer composites are used as electrode materials in supercapacitors [5-7]. Nanoparticles and carbon nanomaterials which have various applications in electrochemistry, photocatalysts, drug delivery, adsorption, and pollutant degradation are also widely used in supercapacitors. Nowadays many articles have been published with the subject of the application of nanotechnology in supercapacitors.

One of the most important carbon materials used in the construction of supercapacitor electrodes is the reduced graphene oxide (rGO). The high-capacity supercapacitors have been made due to the extraordinary surface area of rGO (The capacity of the single-layer rGO is about  $21 \mu\text{Fcm}^{-2}$ ) [8-12]. Since there is a relatively low electrical conductivity of rGO due to oxygenated group and structural defects, the GO should be reduced. The reduction of GO have challenges due to toxicity and corrosiveness. Some problems in the production of rGO are complicated chemical production and purification methods, the high volume of and low pore density [13-19]. One of the reduced GO preparation methods is the reduction of rGO with chemical or thermal treatment. In this work, rGO was prepared by both reduction methods.

Also, various carbon electrodes modified by metal oxides, nanowires, carbon nanotubes, hydrogels, Metal-organic frameworks (MOFs), sulfides, and carbonates have been reported as supercapacitors. The supercapacitors with high capacitance are produced by a combination of rGO with these materials that cover a wide range of semiconductor materials, conductors and insulators. Metal oxides provide high capacitance at low resistances. This good feature of metal oxides accompanied by the fast and reversible redox reaction has led to the use of them in the construction of various supercapacitor electrodes. Metal oxides named quasi-capacitors include ruthenium, nickel, manganese, iron, vanadium, chromium, and other metal oxides. Among these, ruthenium has the highest capacity, but other metal oxides are used instead due to the

high cost of ruthenium and lack of biocompatibility. However, metal oxides have less conductivity and weaker performance than carbon materials. One way to increase the efficiency of metal oxides is to prepare supercapacitors based on metal oxide composites with carbon materials. This improves rapid capacity loss after several cycles which is the most important disadvantageous of metal oxides. Therefore, in this work GO is first synthesized and then reduced by thermal (Th) and chemical (Hydrazine hydrate (HH)) reduction methods. Then, nanocomposite was prepared by mixing chromium oxide ( $\text{Cr}_2\text{O}_3$ ) and rGO. Their supercapacitor properties were investigated. Here, the capacitance of each electrode was investigated by charge and discharge technique.

## **2. EXPERIMENTAL**

### **2.1. Chemicals**

Graphite (99.9%), sulfuric acid (98%), phosphoric acid (85%), potassium permanganate ( $\geq 99\%$ ), N-methyl pyrrolidone (NMP, 99.5%), hydrogen peroxide (30%), hydrochloric acid (37%), hydrazine hydrate (35%), ethanol (absolute), chromium (VI) oxide ( $\text{CrO}_3$ ,  $\geq 98.0\%$ ), and other reagents were purchased from Merck and Sigma Aldrich Co. Ascorbic acid and other solutions were prepared in deionized water.

### **2.2. Synthesis of GO**

Improved Hummers method was used to synthesize GO. In this method, 3 g of graphite (1% wt) was first dispersed in a solvent consisting of 360 mL sulfuric acid (98%) and 40 mL of phosphoric acid (85%) under ultra-sonication for 1 h. Then, 18 g of potassium permanganate (6% wt) was added during 30 min, the solution was then allowed to stir at 50 °C for 24 h. The reaction vessel was placed in an ice-bath and 150 mL of water as well as 4 mL of hydrogen peroxide (30%) was added dropwise until the color of the solution turned. The sediment was separated by centrifugation and then washed three times with 5% hydrochloric acid and five times with distilled water and finally dried in an oven at 60 °C. The obtained powder was named as GO.

### **2.3. Reduction of GO using hydrazine hydrate**

100 mg of GO was initially dispersed in 100 mL of distilled water under ultrasonication for 30 min. 1 mL of HH was then added to the solution. The solution was then refluxed at 90 °C for 24 hours until the color of the solution changed from brown to black. Finally, the black sediment was freeze-dried and washed with distilled water and methanol. Finally, it was dried in an oven at 70 °C. The resulting powder was named as HH.rGO.

#### **2.4. Reduction of GO by a thermal method**

In this method, 100 mg of GO was placed in an oven at 300 °C for 1 h which its temperature increased by 2 °C min<sup>-1</sup>. The obtained black powder was named as Th.rGO.

#### **2.5. Synthesis of Cr<sub>2</sub>O<sub>3</sub>**

10 g CrO<sub>3</sub> and 5.03 g of absolute ethanol were transferred to a beaker consisting of 120 mL distilled water. After homogenizing the mixture using a magnetic stirrer, it was transferred to an autoclave and placed at 190 °C for 1 h. The resulting brown gel was washed several times with distilled water and dried at 60 °C. The resulting samples were calcined at 500 °C and its color changed to dark green.

#### **2.6. Characterization instrumentation**

The crystallographic investigations of the mentioned materials were performed by a Philips XRD instrument model PW-1730 that was equipped with radiation of Cu K $\alpha$  in  $k = 0.15406$  nm. Also, a Zeiss SIGMA field-emission scanning electron microscope, the VP model was applied for studying nanomaterials' structural morphology.

#### **2.7. Electrochemical studies**

To prepare the electrodes, a piece of nickel foam was cut at a ratio of 2 cm  $\times$  1 cm. The cut foams were washed several times with water and acetone and then they were dried. Initially, the active material of Cr<sub>2</sub>O<sub>3</sub>-graphene binary composite was mixed in NMP solvent (with a ratio of 20:80) using ultrasonication for 30 min. The obtained suspension was sprayed onto the nickel foam substrate to deposit the substrate completely. Different conditions including the distance of spray with the substrate, the hot plate temperature, and also the speed of the spraying process were optimized to make the spraying process repeatable. During the film deposition, nickel foam substrates were placed on a heater at 100 °C to evaporate the sprayed solvent. The mass of the electrodes was measured before and after film deposition, and thus the mass deposited was obtained in the range of 1 to 2 mg.

EIS (electrochemical impedance spectroscopy) and CV (cyclic voltammetry) experiments were performed using an Autolab 302N electrochemical workplace containing 3 electrodes, SCE, platinum foil and the modified electrodes with HH.rGO/Cr<sub>2</sub>O<sub>3</sub> and Th.rGO/Cr<sub>2</sub>O<sub>3</sub> nanocomposite as a reference, counter and the working electrodes, respectively. The measurements were done in a 6 M KOH electrolyte at room temperature. CV experiments were performed at a potential range of -0.05 to 0.45 V (versus SCE) at different scan rates. The EIS electrochemical analysis was obtained in the frequency range of 100 kHz to 0.01 Hz at open circuit potential. In the EIS tests, a perturbation with a value of 10 mV AC was applied.

According to the resulted data of CV tests, the SC (special capacity) of the nanocomposite in the structure of working electrodes can be estimated by the given equation:

$$SC = \frac{\int IdV}{vmV} \quad (1)$$

where current density is  $I$  (A), the mass of the electroactive material is  $m$  (g), scan rate and the potential are  $v$  ( $V s^{-1}$ ) and  $V$  (V).

The SC of the electroactive nanocomposite in this study can also be estimated through the resulted data from charge/discharge process by the following equation:

$$SC = \frac{I\Delta t}{\Delta V} \quad (2)$$

$I$ ,  $\Delta t$  and  $V$  represent current, discharge time and the discharge potential in the charge/discharge process in terms of Ampere, the second and Volt, respectively.

### 3. RESULTS AND DISCUSSION

#### 3.1. Characterization

FT-IR is a suitable technique for identifying functional groups and the structure of different compounds [20-26].

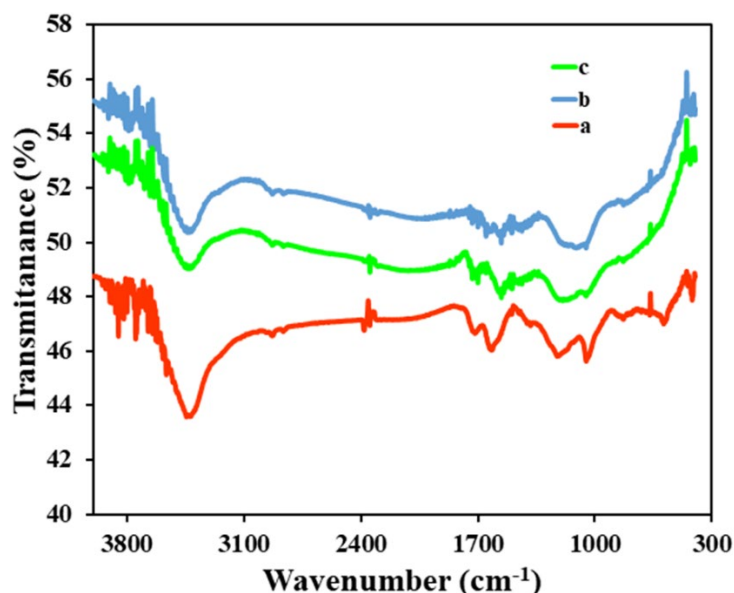
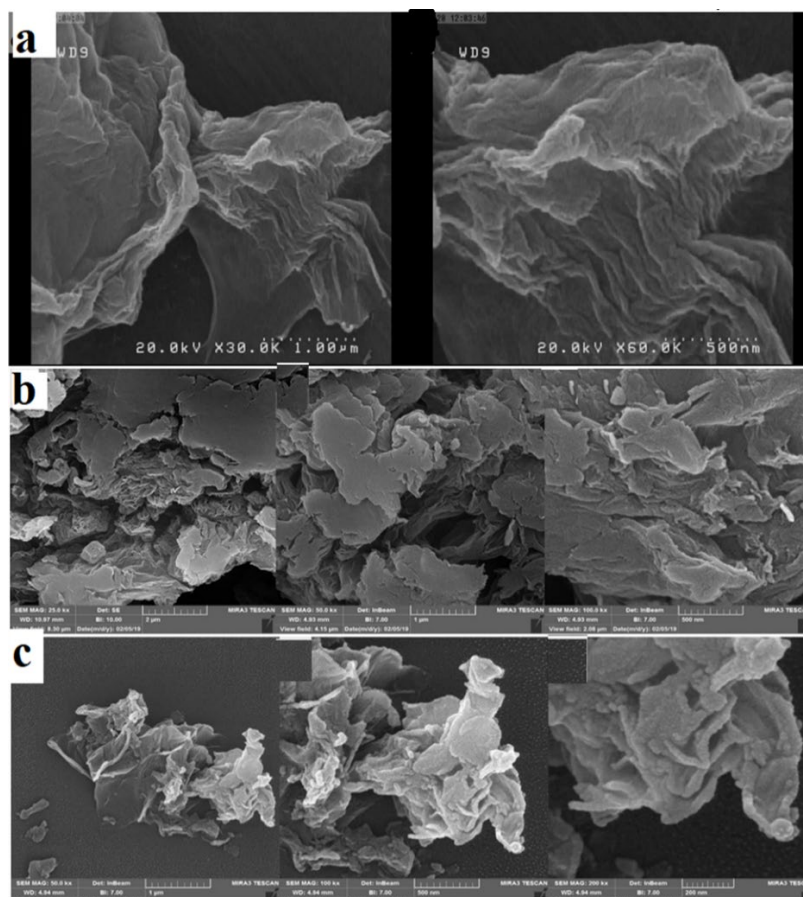


Fig. 1. FTIR spectra of (a) GO, (b) HH.rGO and (c) Th.rGO

Fig. 1a shows the FT-IR spectrum of the synthesized GO. The peaks that appeared in the FT-IR spectrum indicate the presence of oxygen-containing functional groups in the composition. The peaks in the  $3384\text{ cm}^{-1}$ ,  $1735\text{ cm}^{-1}$ , and  $1048\text{ cm}^{-1}$  regions are related to the  $-OH$  group,  $C-OH$  and  $C-O$  bonds, respectively. Given the existence of these groups in the composition, it can be said that

graphite is well-converted to GO. Fig. 1b shows the FT-IR spectrum of HH.rGO. As it is clear, the peaks in the FT-IR spectrum of GO which belonged to oxygen-containing groups have become much weaker or disappeared in this spectrum. This indicates that the GO has been well reduced to graphene. Fig. 1c shows the FT-IR spectrum of rGO prepared by the thermal method. The peaks show that the oxygen-containing groups are well reduced indicating the successful synthesis of rGO.



**Fig. 2.** SEM image of (a) GO, (b) HH.rGO and (c) Th.rGO

Fig. 2a shows the SEM images of the synthesized GO. As it is clear, the layers of GO are completely stacked together. Fig 2b shows the SEM images of HH.rGO at different magnifications. This figure shows that the product consists of the layer with a low thickness which indicates the layered GO stacked together. Fig 2c shows the SEM images of Th.rGO at various magnifications. As it is clear, the product consists of separate layers with low thickness.

XRD is a powerful technique for identifying the structure of crystalline compounds [27-29]. Fig 3a and b show the XRD patterns of the pristine graphite and the synthesized GO. Also, the standard patterns are given in the corner of figures. In the XRD pattern of the GO, the disappearance of the characteristic peak of graphite in the 25-30 ° region and appearance of strong peak an angle of 10 ° and a weak peak in the range of 40 °-45 ° indicate the successful synthesis of GO. Figure 3 c and d also show the XRD patterns of HH.rGO and Th.rGO. Two

weak peaks appeared in regions of 20°-30° and 40°-50° indicate that the GO has been well converted to graphene.

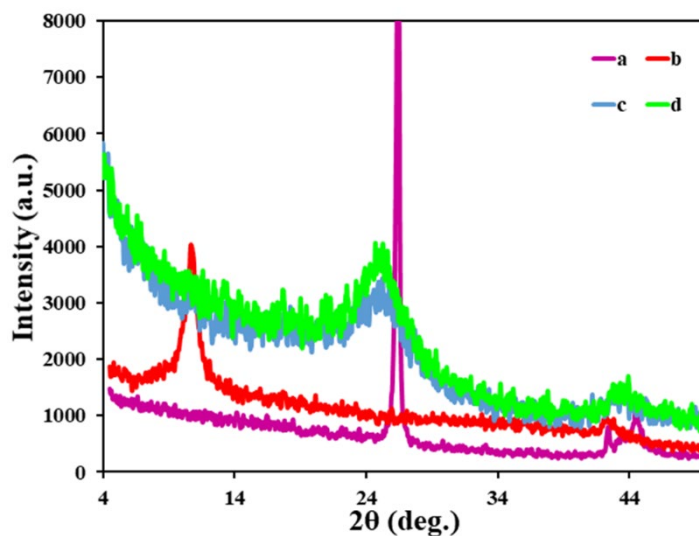


**Fig. 3.** XRD patterns of (a) graphite, (b) GO, (c) HH.rGO and (d) Th.rGO

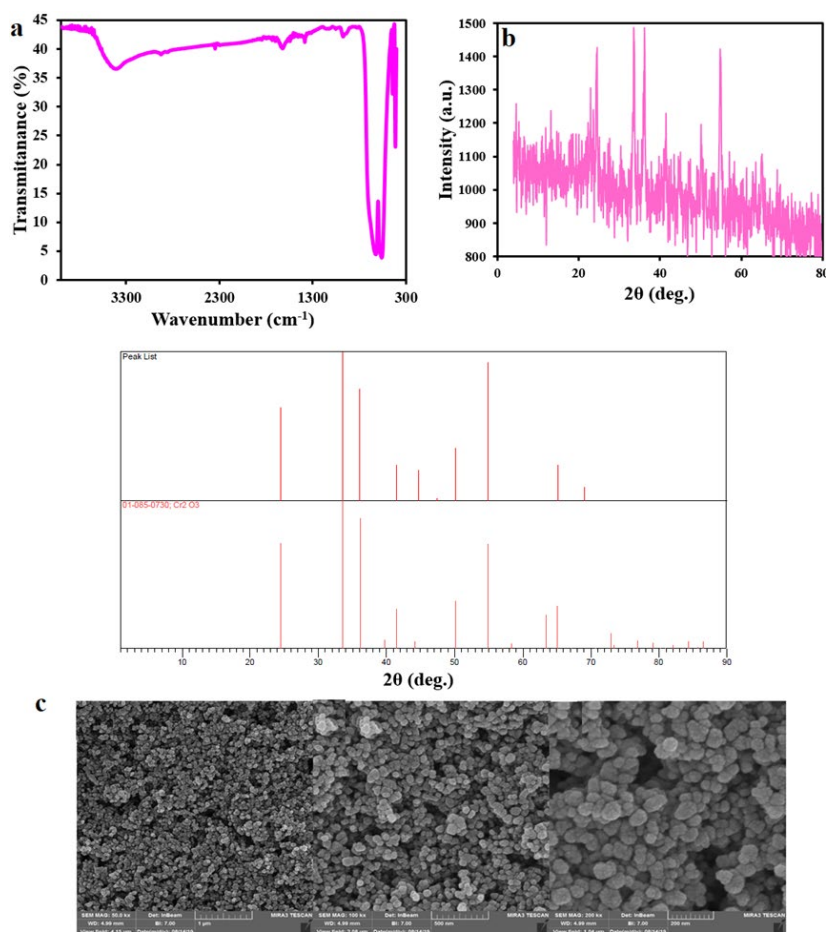
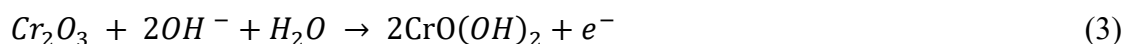


**Fig 4.** (a) FT-IR spectrum, (b) XRD pattern, (c) SEM images and (d) particle size distribution diagram of Cr<sub>2</sub>O<sub>3</sub> nanoparticles

Fig. 4a shows the FT-IR spectrum of Cr<sub>2</sub>O<sub>3</sub> nanoparticles synthesized and calcined at 500 °C. The peaks in the region 500-700 cm<sup>-1</sup> indicate the oxide-metal bond. The appeared peak at 560 cm<sup>-1</sup> is related to Cr–O bending vibration and peak at 624 cm<sup>-1</sup> is attributed to the Cr<sub>2</sub>O<sub>3</sub> phase [74]. Fig. 4b shows the XRD pattern of the calcined Cr<sub>2</sub>O<sub>3</sub> at 500 °C. The obtained pattern corresponds to the standard card No. 01-85-0730 of Cr<sub>2</sub>O<sub>3</sub> and confirms the FT-IR results. Fig. 4c shows the SEM images of the nanostructured Cr<sub>2</sub>O<sub>3</sub> that calcinated at 500 °C. It is clear from these images that the synthesized nanostructure is spherical nanoparticles. The average particle size obtained using digimizer software is 45 nm (Fig. 4d).

### 3.2. Electrochemical studies

The CV test was performed at HH.rGO/Cr<sub>2</sub>O<sub>3</sub> and Th.rGO/Cr<sub>2</sub>O<sub>3</sub> electrode surfaces in the potential window of -0.05 to 0.45 V at the scan rates of 10 to 200 mV s<sup>-1</sup>. According to the results (shown in . 5 a-c), a pair of the oxidation-reduction peak is observed which is related to the conversion between the different oxidation-reduction states of chromium. This pair of the oxidation-reduction peak is observed at about 0.23 V and 0.34 V at a scan rate of 10 mV s<sup>-1</sup> is mainly due to Faraday's reactions between Cr<sup>3+</sup> and Cr<sup>4+</sup>. Faraday's reversible reactions can be done as follows:



The anodic peak becomes more positive and the cathodic peak becomes more negative with the increase in the scan rate which can be attributed to the electrode polarization effects at high scan rates. Besides, the trend of all shapes is maintained even at scan rates of above 200 mV/s but they are slightly disappeared at the higher scan rates. To further investigate, the CV curve at the scan rate of 50 mV s<sup>-1</sup> was plotted for two composite samples of Cr<sub>2</sub>O<sub>3</sub> -graphene and are shown in Fig. 5c. This figure indicates the better performance of the composite of Cr<sub>2</sub>O<sub>3</sub> with graphene reduced by a thermal method.

Fig. 6 a and b show the charge-discharge curves of two composite of HH.rGO/Cr<sub>2</sub>O<sub>3</sub> and Th.rGO/Cr<sub>2</sub>O<sub>3</sub> at various current densities 1-20 A g<sup>-1</sup>. As expected, the discharge time decreases, and the ohmic drop in the system increases with an increase in the discharge current density. The discharge capacity obtained for HH.rGO/Cr<sub>2</sub>O<sub>3</sub> and Th.rGO/Cr<sub>2</sub>O<sub>3</sub> at a current density of 1 A g<sup>-1</sup> are 104.6 and 151.7 F g<sup>-1</sup>, respectively. Accordingly, the special capacity versus current density is plotted in Fig 6c which indicates the superiority of the HH.rGO/Cr<sub>2</sub>O<sub>3</sub> and Th.rGO/Cr<sub>2</sub>O<sub>3</sub> electrode.

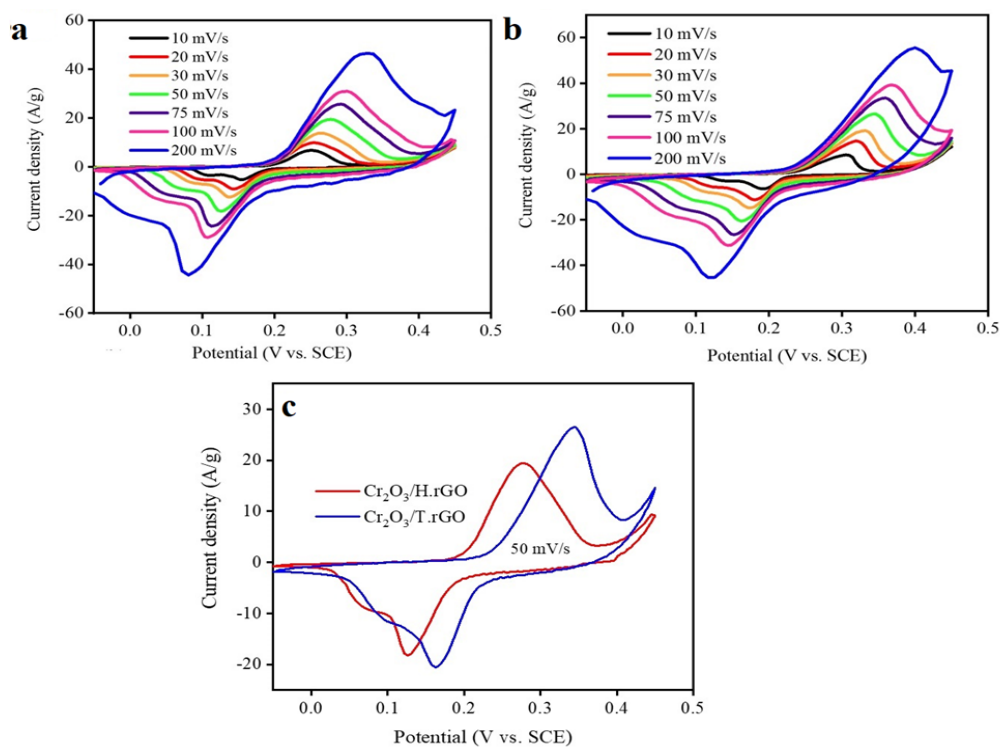


**Fig. 5.** CV plots of (a) HH.rGO/Cr<sub>2</sub>O<sub>3</sub> and Th.rGO/Cr<sub>2</sub>O<sub>3</sub> based electrode at different scan rates, (c) HH.rGO/Cr<sub>2</sub>O<sub>3</sub> and Th.rGO/Cr<sub>2</sub>O<sub>3</sub> based electrodes, at 50 mV s<sup>-1</sup> in 6.0 M KOH as an aqueous electrolyte and (d) specific capacitance as a function of the scan rates for the electrodes constructed with HH.rGO/Cr<sub>2</sub>O<sub>3</sub> and Th.rGO/Cr<sub>2</sub>O<sub>3</sub> nanomaterials

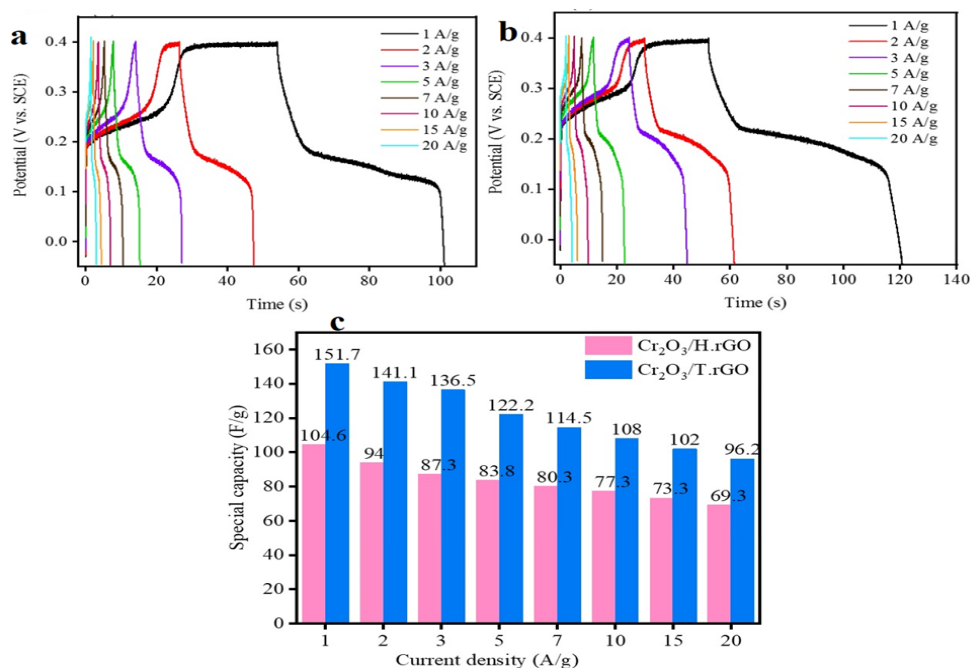


**Fig. 6.** Charge/discharge curves of the HH.rGO/Cr<sub>2</sub>O<sub>3</sub> and Th.rGO/Cr<sub>2</sub>O<sub>3</sub> electrodes at different current densities (a and b), charge/discharge curves of the HH.rGO/Cr<sub>2</sub>O<sub>3</sub> and Th.rGO/Cr<sub>2</sub>O<sub>3</sub> electrodes at current density of 2.0 A g<sup>-1</sup> (c)

Table 1 summarizes a comparison of HH.rGO/Cr<sub>2</sub>O<sub>3</sub> and Th.rGO/Cr<sub>2</sub>O<sub>3</sub> supercapacitors with those of other previously reported rGO or Cr<sub>2</sub>O<sub>3</sub> composites on different substrates in the literature. This comparison clearly shows that the specific capacitance at the prepared rGO/Cr<sub>2</sub>O<sub>3</sub> is higher than other electrodes.

**Table 1.** Comparison of the specific capacitance of HH.rGO/Cr<sub>2</sub>O<sub>3</sub> and Th.rGO/Cr<sub>2</sub>O<sub>3</sub> with other

Electrode	Electrolyte	Specific capacitance (F/g)	References
graphene/MnO <sub>2</sub>	Na <sub>2</sub> SO <sub>4</sub>	150	[36]
MnO/graphene/nickel foam	Na <sub>2</sub> SO <sub>4</sub>	126	[37]
Cr <sub>2</sub> O <sub>3</sub> /MWCNTs	KOH	147	[38]
Cr <sub>2</sub> O <sub>3</sub> /GO	Na <sub>2</sub> SO <sub>4</sub>	100	[39]
Cr <sub>2</sub> O <sub>3</sub>	KOH	140	[40]
HH.rGO/Cr <sub>2</sub> O <sub>3</sub>	KOH	104	This work
Th.rGO/Cr <sub>2</sub> O <sub>3</sub>	KOH	151	This work

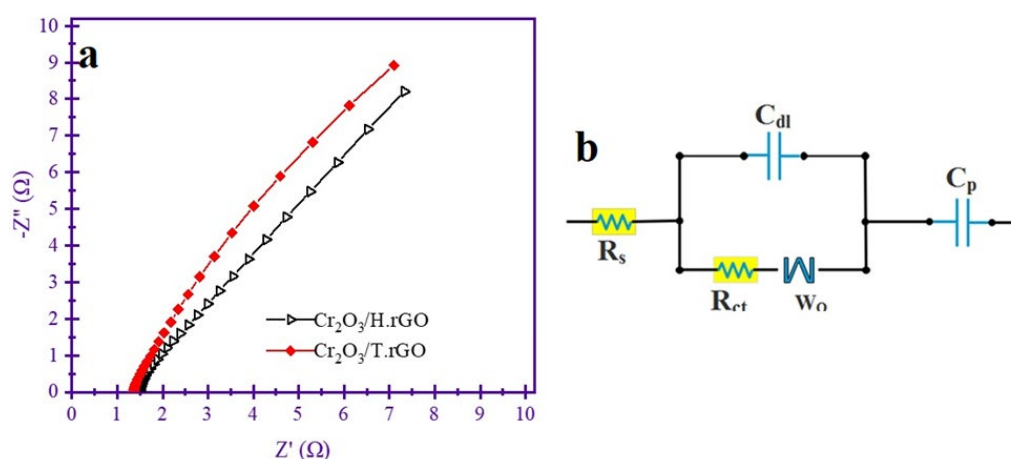


**Fig. 7.** Impedance spectra at a 10 mV amplitude of AC and in 6.0 M KOH electrolyte for HH.rGO/Cr<sub>2</sub>O<sub>3</sub> and Th.rGO/Cr<sub>2</sub>O<sub>3</sub> based electrodes

The Nyquist curve of binary composites has been plotted in Fig 7 a and b. Obtained results are indicated the lower charge transfer resistance of Th.rGO/Cr<sub>2</sub>O<sub>3</sub> relative to Th.rGO/Cr<sub>2</sub>O<sub>3</sub>. Moreover, Warburg slope in the low-frequency range which is the

important factor for charge transfer between electrode and electrolyte. The higher slope of Th.rGO/Cr<sub>2</sub>O<sub>3</sub> indicating the better electrochemical performance of the Cr<sub>2</sub>O<sub>3</sub> nanocomposite with thermally reduced GO [30-35].

#### 4. CONCLUSION

The construction and development of clean energy storage devices have been increased attention over the past few years due to overcoming the problems such as population growth, consequently limited energy supply and environmental problems such as global warming and air pollution. One type of these devices is the supercapacitor. Various electrode materials such as ruthenium oxide and iridium oxide in the metal-oxide family have been used for the development of supercapacitors. Metal oxides such as nickel oxide, manganese oxide, etc. have been introduced as a suitable and low-cost alternative for application in electrochemical supercapacitors compared to expensive ruthenium oxides. In this study, supercapacitors were developed based on composites of Cr<sub>2</sub>O<sub>3</sub> and rGO. The results showed that the maximum capacity with the value of 151.7 F g<sup>-1</sup> was obtained by binary composite based on Cr<sub>2</sub>O<sub>3</sub> and thermally reduced GO.

#### REFERENCES

- [1] K. Adib, M. Rahimi-Nasrabadi, Z. Rezvani, S. M. Pourmortazavi, F. Ahmadi, H. R. Naderi and M. R. Ganjali, *J. Mater. Sci. Mater. Electron.* 27 (2016) 4541.
- [2] S. Sohrabi, and M. Ghalkhani, *J. Electron. Mater.* 48 (2019) 4127.
- [3] S. Sohrabi, M. Ghalkhani, and S. Dehghanpour, *J. Inorg. Organomet. Polym. Mater.* 29 (2019) 528.
- [4] A. Sobhani-Nasab, H. R. Naderi, M. Rahimi-Nasrabadi, and M. R. Ganjali, *J. Mater. Sci. Mater. Electron.* 28 (2019) 8588.
- [5] H. R. Naderi, A. Sobhani-Nasab, M. Rahimi-Nasrabadi and M. R. Ganjali, *Appl. Surf. Sci.* 423 (2017) 1025.
- [6] A. Sobhani-Nasab, M. Rahimi-Nasrabadi, H. R. Nader, V. Pourmohamadian, F. Ahmadi, M. R. Ganjali and H. Ehrlich, *Ultrasonic Sonochem.* 45 (2018) 189.
- [7] H. Reza Naderi, A. Sobhani-Nasab, E. Sohoul, K. Adib and E. Naghian, *Anal. Bioanal. Electrochem.* 12 (2020) 263.
- [8] S. M. Pourmortazavi, M. Rahimi-Nasrabadi, M. Sadeghpour Karimi and S. S. Mirsadeghi, *New J. Chem.* 42 (2018) 19934.
- [9] H. Naderi, A. Sobati, A. Sobhani-Nasab, M. Rahimi-Nasrabadi, M. Eghbali-Arani, M. R. Ganjali and H. Ehrlich, *Chemistry Select* 4 (2019) 2862.
- [10] B. A. H. Zaidan, E. Sohoul, and S. Mazaheri, *Anal. Bioanal. Electrochem.* 11 (2019) 108.

- [11] T. H. Sanatkar, A. Khorshidi, E. Sohoul, and J. Janczak, *Inorganica Chim. Acta* 506 (2020) 119537.
- [12] E. Naghian, and E. Sohoul, *Anal. Bioanal. Electrochem.* 12 (2020) 458.
- [13] E. Naghian, F. Shahdost-fard, E. Sohoul, V. Safarifard, M. Najafi, M. Rahimi-Nasrabadi, and A. Sobhani-Nasab, *Microchem. J.* (2020) 104888.
- [14] J. Amani, A. Khoshroo and M. Rahimi-Nasrabadi, *Mikrochim Acta* (2018) 185.
- [15] M. Rahimi-Nasrabadi, M. Rostami, F. Ahmadi, A. Fallah Shojaie and M. Delavar Rafiee, *J. Mater. Sci. Mater. Electron.* 27 (2016) 11940.
- [16] A. Sobhani-Nasab, S. Behvandi, M. A. Karimi, E. Sohoul, M. Sadeghpour Karimi, N. Gholipour, F. Ahmadi and M. Rahimi-Nasrabadi, *Ceram. Int.* 45 (2019) 17847.
- [17] M. Rostami, M. Rahimi-Nasrabadi, M. R. Ganjali, F. Ahmadi, M. Fallah Shojaei and M. Delavar Rafiee. *J. Mater. Sci.* 52 (2017) 7008.
- [18] M. Gholami, M. A. Salmasi, E. Sohoul, B. Torabi, M. R. Sohrabi and M. Rahimi-Nasrabadi, *J. Photochem. Photobiol. A* (2020) 112523.
- [19] S. Ghasemi, S. Hosseini, and F. Mousavi, *Colloids Surf. A Physicochem. Eng. Asp.* 520 (2017) 477.
- [20] S. M. Pourmortazavi, S. S. Hajimirsadeghi, and M. Rahimi-Nasrabadi, *Mater Sci Semicond Process.* 16 (2013) 131.
- [21] S. M. Peymani-Motlagh, A. Sobhani-Nasab, M. Rostami, H. Sobati, M. Eghbali-Arani, M. Fasihi-Ramandi, M. R. Ganjali and M. Rahimi-Nasrabadi, *J. Mater. Sci. Mater. Electron.* 30 (2019) 6902.
- [22] A. Sobhani-Nasab, M. Behpour, M. Rahimi-Nasrabadi, F. Ahmadi, and S. Pourmasoud, *J. Mater. Sci. Mater. Electron.* 30 (2019) 5854.
- [23] M. Rahimi-Nasrabadi, S. M. Pourmortazavi, M. Aghazadeh, M. R. Ganjali, M. Sadeghpour Karimi and P. Norouzi, *J. Mater. Sci. Mater. Electron.* 28 (2017) 9478.
- [24] M. Rahimi-Nasrabadi, V. Pourmohamadian, M. Sadeghpour Karimi, H. R. Naderi, M. A. Karimi, K. Didehban and M. R. Ganjali, *J. Mater. Sci. Mater. Electron.* 28 (2017) 12391.
- [25] E. Naghian, E. M. Khosrowshahi, E. Sohoul, F. Ahmadi, M. Rahimi-Nasrabadi, and V. Safarifard, *New J. Chem.* (2020).
- [26] M. Rahimi-Nasrabadi, S. M. Pourmortazavi, M. Aghazadeh, M. R. Ganjali, M. Sadeghpour Karimi and P. Novrouzi, *J. Mater. Sci. Mater. Electron.* 28 (2017) 5574.
- [27] M. Rahimi-Nasrabadi, F. Ahmadi, and M. Eghbali-Arani, *J. Mater. Sci. Mater. Electron.* 27 (2016) 13294.
- [28] M. Rahimi-Nasrabadi, F. Ahmadi and M. Eghbali-Arani, *J. Mater. Sci. Mater. Electron.* 28 (2017) 2415.
- [29] M. Rahimi-Nasrabadi, A. Ghaderi, H. R. Banafshe, M. Eghbali-Arani, M. Akbari, S. Pourmasoud and A. Sobhani-Nasab, *J. Mater. Sci. Mater. Electron.* 30 (2019) 15854.

- [30] E. Sohoulı, A. H. Keihan, F. Shahdost-fard, E. Naghian, M. E. Plonska-Brzezinska, M. Rahimi-Nasrabadi and F. Ahmadi, *Mater. Sci. Eng.* 110 (2020) 110684
- [31] S. Shahrokhian, and M. Ghalkhani, *Electrochim. Acta* 51 (2006) 2599.
- [32] E. Sohoulı, M. S. Karimi, E. Khosrowshahi, M. Rahimi-Nasrabadi, and F. Ahmadi, *Measurement* (2020) 108140.
- [33] E. Sohoulı, F. Shahdost-Fard, M. Rahimi-Nasrabadi, M. E. Plonska-Brzezinska, and F. Ahmadi, *Electroanal. Chem.* (2020) 114309.
- [34] F. Mousavi, M. Shamsipur, A. A. Taherpour, and A. Pashabadi, *Electrochim. Acta* 308 (2019) 373.
- [35] F. Mousavi and A. A. Taherpour, *Electrochim. Acta* 318 (2019) 617.
- [36] G. Yu, L. Hu, N. Liu, H. Wang, M. Vosgueritchian, Y. Yang, and Z. Bao, *Nano Lett.* 11 (2011) 4438.
- [37] Y. Q. Zhao, D. D. Zhao, P. Y. Tang, Y. M. Wang, C. L. Xu and H. L. Li, *Mater. Lett.* 76 (2012) 127.
- [38] B. Chen, Y. Wang, C. Li, L. L. Fu, X. Liu, Y. Zhu, and J. Wu, *RSC advances* 7 (2014) 25019.
- [39] P. Asen, and S. Shahrokhian, *J. Electroanal. Chem.* 823 (2018) 505.
- [40] I. Shafi, and E. Liang, *J. Alloys Compd.* (2020) 156046.